Underwater Image Dehazing with a Light Field Camera

Katherine A. Skinner and Matthew Johnson-Roberson
University of Michigan, Ann Arbor
{kskin, mattjr}@umich.edu

Abstract

Underwater vision is subject to effects of underwater light propagation that act to absorb, scatter, and attenuate light rays between the scene and the imaging platform. Backscattering has been shown to have a strong impact on underwater images. As light interacts with particulate matter in the water column, it is scattered back towards the imaging sensor, resulting in a hazy effect across the image. A similar effect occurs in terrestrial applications in images of foggy scenes due to interaction with the atmosphere. Prior work on multi-image dehazing has relied on multiple cameras, polarization filters, or moving light sources. Single image dehazing is an ill-posed problem; proposed solutions rely on strong priors of the scene. This paper presents a novel method for underwater image dehazing using a light field camera to capture both the spatial and angular distribution of light across a scene. First, a 2D dehazing method is applied to each sub-aperture image. These dehazed images are then combined to produce a smoothed central view. Lastly, the smoothed central view is used as a reference to perform guided image filtering, resulting in a 4D dehazed underwater light field image. The developed method is validated on real light field data collected in a controlled in-lab water tank, with images taken in air for reference. This dataset is made publicly available.

1. Introduction

Underwater image formation is a complex physical process due to the effects of light propagation through an aqueous medium. As a photon of light travels between a camera and the target scene, it interacts with particulate matter in the water column and can be scattered or absorbed. This results in images often blue-green in color as the red wavelength is absorbed at the highest rate. Light that is scattered back towards the camera – backscattering – adds a hazy effect to underwater images (Fig. 1). These effects are range-dependent and thus restrict image capture to a typical range of $1 - 2m$ from the seafloor. This necessitates the use of robotic platforms that can carefully follow the terrain

to keep within the focus range of imaging sensors. Since ambient light is limited in the deep sea, artificial lighting is relied on for these surveys. All of these characteristics of underwater image formation and restrictions for data collection pose unique challenges to the field of computer vision. Development of robust methods that compensate for these effects enables success in a range of marine applications [13, 9].

Figure 1. Underwater image subject to effects of underwater light propagation. Note the haze effect across the scene. This is due to backscattering, which acts to add light back to the image sensor [1].

Light field cameras offer solutions to many of these challenges. Light field cameras capture both the spatial and angular distribution of light for a 4D parametrization of the imaged light field. Since this is a single, passive optical sensor, it can operate underwater at close range with artificial lighting. Multiple views are captured simultaneously to enable computation of a depth map from a single frame. Additionally, the 4D parametrization allows for refocusing and extended depth-of-field, relaxing restrictions for underwater vehicles attempting to closely follow the seafloor. Still, challenges associated with underwater light propagation hinder the ability to use existing methods for light field processing on underwater images due to degradation of image appearance from backscattering and attenuation. There is limited literature on compensating for effects of underwater image formation with a light field camera. Additionally,

there is a lack of openly available datasets of underwater light field imagery. Addressing these challenges would enable current methods of light field processing used in air to be transferred to the underwater domain.

The main contributions of this paper are (i) to develop a robust pipeline for dehazing underwater images by exploiting the structure and information provided by a single light field image, and (ii) to provide a comprehensive light field dataset for underwater image dehazing, including light field images of target objects taken in pure water, and in water with different concentrations of particulate matter to produce varying degrees of haze. Images taken in air are also provided for reference.

This paper is presented in the following sections: Section 2 presents prior work, Section 3 details our technical approach, and Section 4 describes the experimental setup and our results. Finally, Sections 5 and 6 discuss these results and conclude with suggestions for future work.

2. Previous Work

Prior work on image dehazing can be separated into either single or multi-image approaches. Methods for multiple views have relied on images taken in different conditions, such as in different weather conditions [18], or using polarization filters [22]. Single image dehazing is an ill-posed problem. He et al. developed the Dark Channel Prior (DCP) to estimate transmission maps of natural scenes for dehazing in terrestrial applications [11]. Fattal leveraged a statistical model of image formation, the color line model, to compute transmission maps more consistent with physical expectation [8]. Several methods have also addressed the issue of non-uniform illumination that arises in scenes imaged at night [16, 2, 28].

Methods for both multi- and single image dehazing have been extended to work in underwater environments. Multi-image methods again rely on images taken under different conditions, such as polarization [21], or under different lighting, such as in photometric stereo [26, 20, 17]. Other methods take into account information available from an underwater imaging survey, such as lighting configuration and vehicle range from the seafloor [3]. For single image dehazing underwater, Drews et al. extended the DCP to the Underwater Dark Channel Prior (UDCP) [7]. Carlevaris et al. developed a novel prior exploiting the difference between color channels of underwater images due to attenuation [4]. Recently, several deep learning approaches have also been proposed for underwater image restoration [23, 15].

Skinner and Johnson-Roberson have previously proposed a method for 3D reconstruction of underwater scenes with a light field camera, but this method was tested in pure water and did not address compensation for scattering apparent in environments with murky water [24]. Dansereau

et al. demonstrated the potential for using light field cameras in underwater dehazing through work focused on the design of a 4D hyperfan filter for volumetric focus of light field images [6]. For dehazing, Dansereau et al. performed gain-adjustment on input images, which does not account for the range-dependent effects of underwater image formation. Our proposed method directly accounts for these effects using a physical model. A key advantage to a physically-based approach is that structural information is inherently embedded in the process of underwater image formation. Thus, we not only recover a dehazed image but also an estimate for transmission of the scene, which is range-dependent.

3. Technical Approach

Throughout this section we use a two-plane parametrization of a light field image to provide the 4D structure $L(x, y, u, v)$, where (u, v) denotes angular coordinates and (x, y) denotes spatial coordinates [25]. Sub-aperture images are obtained by holding angular coordinates constant across the 4D light field such that the center sub-aperture image is given by $L(x, y, 0, 0)$. Algorithm 1 outlines our proposed method for compensating for backscattering in underwater light field images, which takes a hazy light field image $L(x, y, u, v)$ as input and produces the dehazed 4D light field $\widetilde{L}(x, y, u, v)$ as output. The remainder of the section provides further details for each step.

Algorithm 1 Proposed approach for dehazing an underwater light field image.

Input: $L(x, y, u, v)$
Output: $\widetilde{L}(x, y, u, v)$
 1: $J(x, y, u, v) \leftarrow \text{InitialDehaze}(L(x, y, u, v))$
 2: $\widetilde{J} \leftarrow \text{SynthesizeViews}(J(x, y, u, v))$
 3: $\widetilde{L}(x, y, u, v) \leftarrow \text{GuidedImageFiltering}(\widetilde{J}, J(x, y, u, v))$
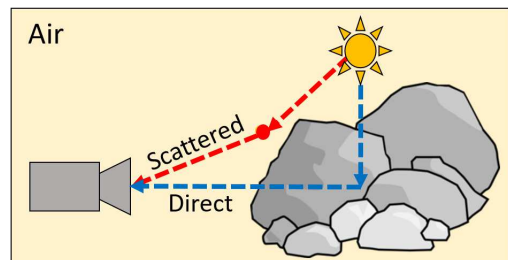

3.1. Dehazing Model

Figure 2. Abstraction of direct and scattered components of image formation model for a terrestrial scene in daylight.

We will start with the base model for dehazing of single

images in terrestrial applications and describe an extended model applicable to underwater dehazing of single images. The base model accounts for both direct transmission of light from a target object and light that does not reach the target object, but instead interacts with particulate matter in the atmosphere and is scattered towards the camera to produce a fog or haze effect (Fig. 2). This model is given by:

$$I(\mathbf{x}) = J(\mathbf{x})t(\mathbf{x}) + (1 - t(\mathbf{x}))A, \qquad (1)$$

where $\mathbf{x}$ denotes spatial coordinates of a single image, $J(\mathbf{x})$ is the true irradiance of the scene, $I(\mathbf{x})$ is the observed image, A is environmental or ambient light, and $t(\mathbf{x})$ is transmission, which is related to range d between the camera and the scene by

$$t(\mathbf{x}) = e^{-\eta d(\mathbf{x})}. \qquad (2)$$

Here η is a scalar attenuation coefficient. Note that when considering the complete model of underwater image formation, attenuation of light occurs due to compounding effects of scattering and absorption, which is wavelength-dependent. When discretized into red, green, and blue color channels, the wavelength-dependent coefficient $\eta(\lambda)$ is highest for the red channel leading to disproportionate attenuation of red compared to blue and green channels in images. In this work, we focus on the problem of dehazing, or correcting for the effects of backscattering only. Thus we use a constant coefficient η across each wavelength as modeled in prior work on underwater image dehazing [4].

One assumption this model makes is that environmental light, A is constant across a scene. This is realistic for a foggy terrestrial scene taken in daylight, where sunlight is the main source of ambient lighting. This assumption does not hold for typical configurations of underwater surveys, especially in the deep ocean where ambient lighting is limited and artificial lighting is required. The artificial light causes non-uniform illumination across the imaged scene, often resulting in hotspots or glow where the light beam is directly pointing (Fig. 3).
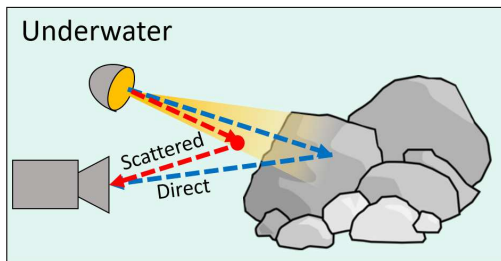

Figure 3. Abstraction of direct and scattered components of image formation for an underwater scene with artificial lighting.

This scenario also occurs in images taken at night. Li et al. proposed an extended model for nighttime haze removal that corrects for glow and non-uniform illumination across a scene imaged at night [16]:

$$I(\mathbf{x}) = J(\mathbf{x})t(\mathbf{x}) + (1 - t(\mathbf{x}))A(\mathbf{x}) + L_a(\mathbf{x}) * APSF, \qquad (3)$$

where $*$ denotes a convolution. Now $A(\mathbf{x})$ varies across the image to account for non-uniform illumination across the scene. $APSF$ is the atmospheric point spread function used to model glow in images [19]. L_a denotes an active light source. Note that for nighttime dehazing, this model is used to account for point source lights that appear within a scene. In underwater image dehazing, glow more often occurs due to the beam pattern of artificial lights used to illuminate the scene at close range. This direct lighting results in a hotspot in the image that produces the brightest illumination in the center of the light beam with decreasing brightness spread radially away from the center. However, this model is generalizable to other cases where lighting from a nearby vehicle or diver also appears in the scene.

We employ this extended model across each sub-aperture image to obtain an initial estimate of the dehazed light field image $J(x, y, u, v)$. For details of the solution, the reader is referred to the original paper [16].

3.2. Synthesizing Views

After this step, we note that the individually dehazed sub-aperture images still contain noise, which is not consistent across sub-aperture images. By averaging across multiple images, much of this noise can be suppressed. We take the mean of dehazed sub-aperture images to form an improved estimate of the center sub-aperture image, $\widetilde{J}$. This assumes that the depth variation across the scene is reasonably small. The following subsection discusses our approach to extend denoising to the full 4D light field structure. Fig. 4 shows the center view sub-aperture image with initial dehazing compared to the synthesized view.

3.3. Recovering Epipolar Images

Using the multiple views provided by the light field image, we have recovered a dehazed image with improved quality compared to the initial dehazing estimate. However, this dehazed image represents the center view only. We wish to recover additional sub-aperture images with improved quality while preserving the important details of $\widetilde{J}$. To do this, we use a guided image filter [12]. The guided image filter takes as input the image to be filtered and a reference or guidance image that contains desired details for preservation. We smooth each dehazed sub-aperture image based on the input guidance image, $\widetilde{J}$. To account for the translational shift across sub-aperture images, we register $\widetilde{J}$

Figure 4. Comparison of initial dehazed center sub-aperture image (left) and the synthesized view $\widetilde{J}$ (right).

to each sub-aperture image prior to filtering. Fig. 5 shows the final result of the center view with recovered epipolar images.
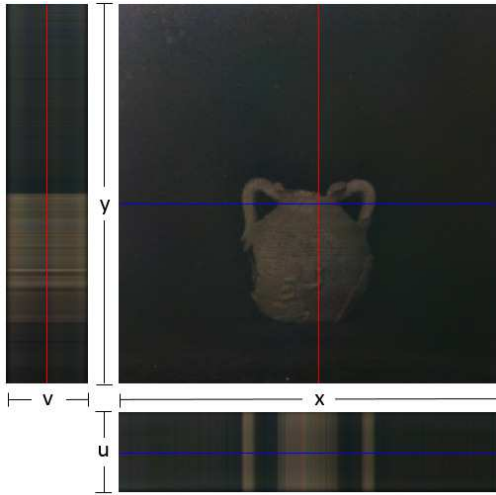

Figure 5. Final result of the center view of the dehazed image with recovered epipolar images.

4. Experiments & Results

4.1. Experimental Setup

We validated our proposed method in a controlled lab setting (Fig. 6). Our setup features an acrylic water tank with dimensions $18in. \times 18in. \times 36in.$ The tank is lined with opaque black fabric to prevent reflection of light from the tank walls. Total internal reflection at the water-air interface is neglected. The tank is placed in a dark room to limit global lighting effects. An underwater light is placed in the tank to provide a single source of direct light, which is a realistic scenario for a deep ocean imaging surveys. To simulate conditions for backscattering encountered in open-sea field experiments, milk was added to the tank to provide suspended particulate matter for increased scattering

Figure 6. Experimental setup with in-lab water tank in controlled lighting environment with a single direct lighting source. The light field camera is placed flush to the tank wall for imaging an artificial scene a distance of approximately $1m$ from the camera. Milk is added to the pure water tank to simulate effects of backscattering present in field experiments.

effects. Target objects were placed at the end of the tank, a maximum of $36in.$ from the camera, and imaged with a Lytro First Generation camera fixed at the other end of the tank, with the tank side acting as a flat viewport. To decode the raw image from the Lytro camera, we followed the decoding process outlined in [5].

4.2. Results

Fig. 7 shows the results of our pipeline for five target objects. The left image shows a high-resolution image taken in air for visual reference. Next is the raw underwater image taken with a Lytro light field camera in murky water conditions. This demonstrates the degradation typical of underwater images taken in field tests, where the haze effect dominates the image. The initial estimate of dehazing based on (3) for single sub-aperture images is provided. This initial estimate shows color distribution closer to the expected distribution in air, however a noise pattern is still visible in the individual images. The final image is the result of our proposed method after synthesizing views and performing guided image filtering. The resulting images have reduced noise and maintain the details of the imaged objects. Note that these are the center images of each light field image and the full 4D structure is preserved for the final result.

To validate our choice of dehazing model, we compare our results for initial dehazing with another method that uses a physical model for image formation to perform single image dehazing underwater [7]. This method uses the base model of single image dehazing in (1) with a statistical prior based on underwater images, the underwater dark channel prior (UDCP). Fig. 8 shows this comparison with the top images produced from single image dehazing using our initial dehazing model and the bottom row showing single images dehazed with UDCP. For UDCP we used a patch size of 15 as recommended by the authors. Note that UDCP does not account for non-uniform illumination across the
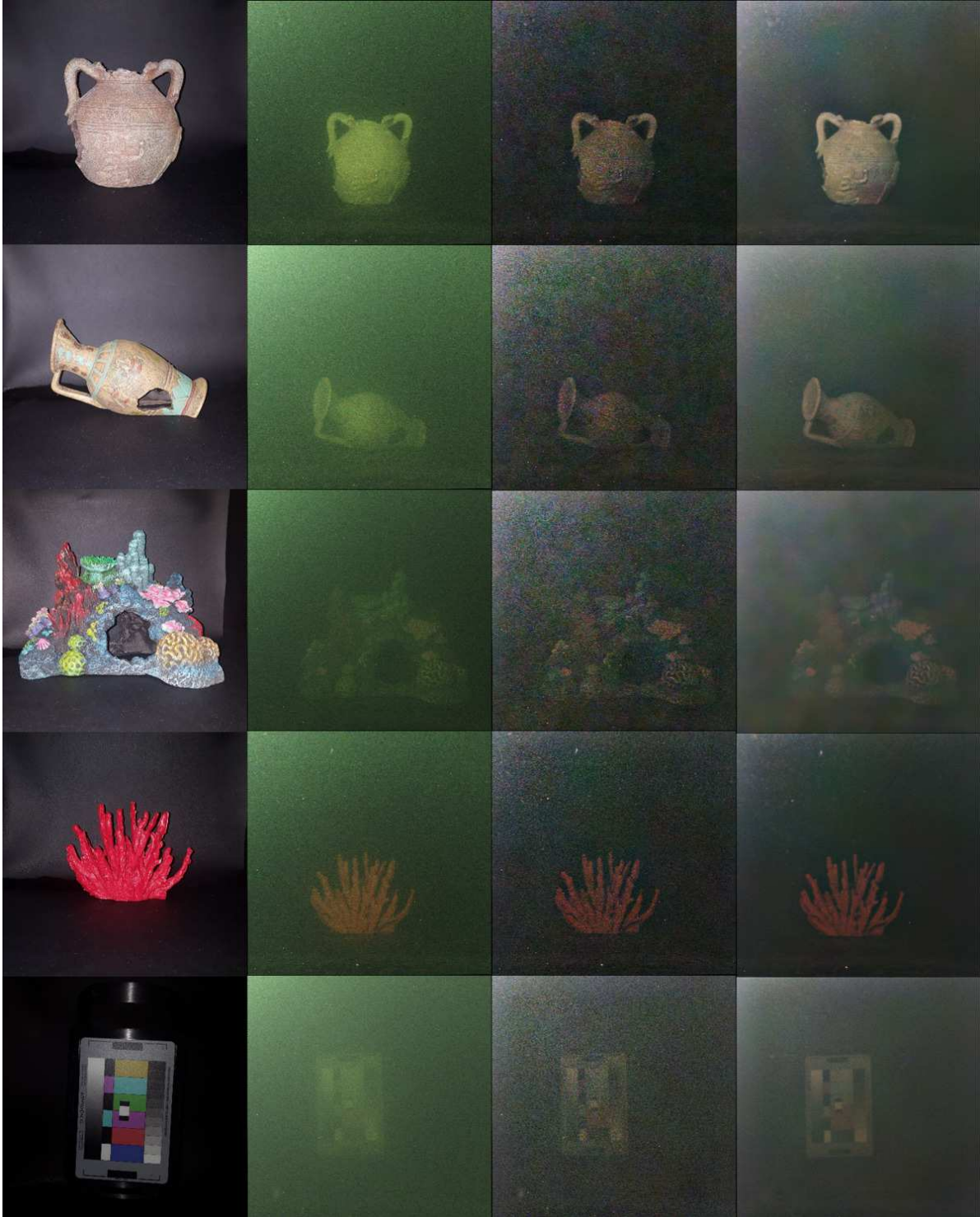
Figure 7. From left to right: Ground truth target imaged in air, raw image underwater, initial estimate of dehazed image, result of dehazed image with guided image filter using the registered synthesized view as a guidance image.

scene or for glow patterns in the image. Instead this method uses a global estimate for environmental light, A. Our initial dehazing step provides a consistent result across different images, whereas results using UDCP can show a color bias in regions of an image due to the assumption of uniform illumination and constant environmental light across a scene.

Lastly, to evaluate the improvement from the hazy image to the dehazed image, we show an estimation of disparity for a light field image of the scene in pure water (no milk added) for reference, the hazy light field imaged in murky water, and the dehazed light field using our proposed pipeline (Figs. 9 - 11, respectively). Sparse disparity maps are estimated using the open-source light field suite software, cocolib [10, 27]. These sparse disparity maps are then interpolated using a matting Laplacian for a smoother estimate [14]. Results are normalized between 0 and 1. These results show that the degradation of raw underwater images taken in murky water also causes degradation of disparity estimation when compared to processing of light field images captured in pure water. Our proposed method recovers enough information within the 4D light field structure to improve disparity estimation.

5. Discussion

Overall, our results demonstrate the potential for using light field cameras in underwater perception tasks. Dehazing of underwater images is a challenging computer vision problem as information is lost about the scene due to degradation of images and occlusion of image points by floating particulate matter in the water column. However, the multiple views captured by a light field camera carry enough information to recover much of the information that is lost in a single image.

The dataset presented here is made publicly available. [1] The dataset contains underwater light field images in pure water and hazy conditions, as well as images taken in air for reference. Future work will extend this dataset to feature greater depth variation and varying levels of turbidity to provide a stronger benchmark for testing developed methods.

Future work will also focus on further exploiting the structure provided by light field cameras to overcome limitations of our proposed approach. In particular, taking the mean of sub-aperture images can introduce blur for scenes with large depth variation. Incorporating all-in-focus filters that overcome this issue and preserve the full depth-of-field is a promising next step. Since our method is based on a physical model of range-dependent lighting effects, we not only recover a dehazed image but also an estimate for transmission of the scene, which is dependent on range and a

constant attenuation coefficient. Estimation of this coefficient would lead to an estimate for the depth map of the scene. Incorporating the structural information inherently embedded in the physical model of underwater lighting effects is another promising direction for future work.

6. Conclusion

This paper has presented a novel pipeline for dehazing of underwater images taken with a light field camera based on a physical model of underwater light propagation. We also present a comprehensive dataset of murky underwater images taken with a light field camera, including images taken in pure water and in air for ground truth and visual reference. Our results demonstrate improvement from the raw underwater light field image to the final dehazed light field image, and we show that this improvement enables the application of light field processing methods developed for in air applications to be used with images taken underwater. Future work will focus on improving our model for underwater dehazing to more accurately account for underwater lighting effects including wavelength-dependent effects in attenuation. Additionally, focus will be placed on recovering metrically accurate depth maps of the scene. Lastly, we wish to test these methods on more complex scenes with greater depth variation and occlusions to work towards achieving a robust method for light field processing in underwater environments.

Acknowledgement

References

[1] Noaa and partners to survey ships sunk off north carolina in world war ii. *National Oceanic and Atmospheric Administration*, 2009.

[2] C. Ancuti, C. O. Ancuti, C. D. Vleeschouwer, and A. C. Bovik. Night-time dehazing by fusion. In *Proceedings of the IEEE International Conference on Image Processing*, pages 2256–2260, Sept. 2016.

[3] M. Bryson, M. Johnson-Roberson, O. Pizarro, and S. B. Williams. True color correction of autonomous underwater vehicle imagery. *Journal of Field Robotics*, 33(6):853–874, 2016.

[4] N. Carlevaris-Bianco, A. Mohan, and R. M. Eustice. Initial results in underwater single image dehazing. In *Proceedings of the IEEE/MTS OCEANS Conference and Exhibition*, pages 1–8, 2010.

[5] D. G. Dansereau, O. Pizarro, and S. B. Williams. Decoding, calibration and rectification for lenselet-based plenoptic cameras. In *Proceedings of the IEEE Conference on Computer Vision and Pattern Recognition*, pages 1027–1034, 2013.

---

[1] https://github.com/kskin/data

Figure 8. (Top) Intermediate results of our proposed method showing single image dehazing of center sub-aperture image. (Bottom) Comparative results of UDCP, a single image dehazing method based a physical model of image formation underwater.
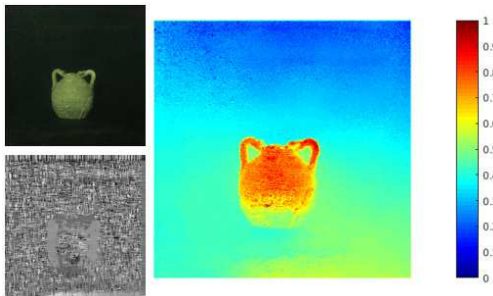

Figure 9. (Top Left) Center view of a light field image taken in pure water. (Bottom Left) Sparse disparity estimate. (Right) Disparity estimate based on a light field image taken in pure water.
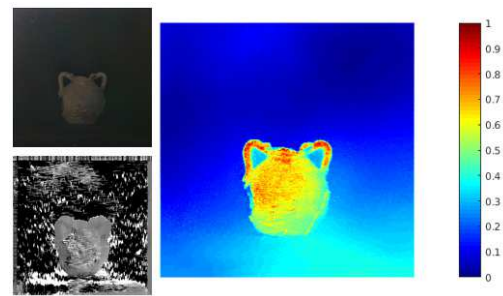

Figure 11. (Top Left) Center view of the dehazed light field image using our proposed method. (Bottom Left) Sparse disparity estimate. (Right) Disparity estimate based on a dehazed light field image using our proposed method.
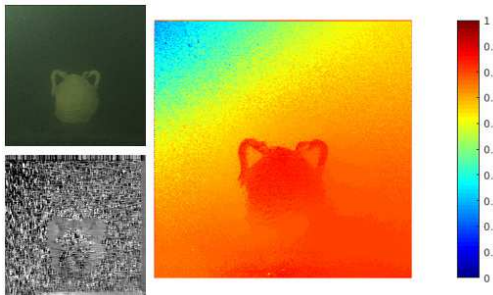

Figure 10. (Top Left) Center view of a light field image taken in murky water. (Bottom Left) Sparse disparity estimate. (Right) Disparity estimate based on a light field image taken in murky water.

[6] D. G. Dansereau, O. Pizarro, and S. B. Williams. Linear volumetric focus for light field cameras. *ACM Transactions on Graphics*, 34(2):15–1, 2015.

[7] P. Drews-Jr, E. do Nascimento, F. Moraes, S. Botelho, M. Campos, R. Grande-Brazil, and B. Horizonte-Brazil. Transmission estimation in underwater single images. In *Proceedings of IEEE International Conference on Computer Vision - Workshop on Underwater Vision*, pages 825–830, 2013.

[8] R. Fattal. Dehazing using color-lines. *ACM Transactions on Graphics*, 34(1):13:1–13:14, Dec. 2014.

[9] R. Gibson, R. Atkinson, and J. Gordon. A review of underwater stereo-image measurement for marine biology and ecology applications. *Oceanography and Marine Biology: An Annual Review*, 47:257–292, 2009.

[10] B. Goldluecke, E. Strekalovskiy, and D. Cremers. The natural vectorial total variation which arises from geometric measure theory. *SIAM Journal on Imaging Sciences*, pages 537–563, 2012.

[11] K. He, J. Sun, and X. Tang. Single image haze removal using dark channel prior. In *Proceedings of the IEEE Conference on Computer Vision and Pattern Recognition*, pages 2341–2353, 2009.

[12] K. He, J. Sun, and X. Tang. Guided image filtering. In *Proceedings of the 11th European Conference on Computer Vision: Part I*, ECCV'10, pages 1–14, 2010.

[13] M. Johnson-Roberson, M. Bryson, A. Friedman, O. Pizarro, G. Troni, P. Ozog, and J. C. Henderson. High-resolution underwater robotic vision-based mapping and three-dimensional reconstruction for archaeology. *Journal of Field Robotics*, pages 625–643, 2016.

[14] A. Levin, D. Lischinski, and Y. Weiss. A closed form solution to natural image matting. In *Proceedings of the IEEE Conference on Computer Vision and Pattern Recognition*, CVPR '06, pages 61–68, 2006.

[15] J. Li, K. A. Skinner, R. M. Eustice, and M. Johnson-Roberson. Watergan: Unsupervised generative network to enable real-time color correction of monocular underwater images. *arXiv preprint arXiv:1702.07392*, 2017.

[16] Y. Li, R. T. Tan, and M. S. Brown. Nighttime haze removal with glow and multiple light colors. In *Proceedings of the IEEE International Conference on Computer Vision*, pages 226–234, 2015.

[17] Z. Murez, T. Treibitz, R. Ramamoorthi, and D. Kriegman. Photometric stereo in a scattering medium. In *Proceedings of the 2015 IEEE International Conference on Computer Vision*, ICCV '15, pages 3415–3423, 2015.

[18] S. G. Narasimhan and S. K. Nayar. Contrast restoration of weather degraded images. *IEEE Transactions on Pattern Analysis and Machine Intelligence*, 25(6):713–724, 2003.

[19] S. G. Narasimhan and S. K. Nayar. Shedding light on the weather. In *Proceedings of the IEEE Conference on Computer Vision and Pattern Recognition*, volume 1, pages 665–672, June 2003.

[20] S. G. Narasimhan, S. K. Nayar, B. Sun, and S. J. Koppal. Structured light in scattering media. In *Proceedings of the IEEE International Conference on Computer Vision*, volume 1, pages 420–427, 2005.

[21] Y. Y. Schechner and N. Karpel. Recovery of underwater visibility and structure by polarization analysis. *IEEE Journal of Oceanic Engineering*, 30(3):570–587, July 2005.

[22] Y. Y. Schechner, S. G. Narasimhan, and S. K. Nayar. Instant dehazing of images using polarization. In *Proceedings of the IEEE Conference on Computer Vision and Pattern Recognition. CVPR 2001*, volume 1, pages 325–332, 2001.

[23] Y.-S. Shin, Y. Cho, G. Pandey, and A. Kim. Estimation of ambient light and transmission map with common convolutional architecture. In *Proceedings of the IEEE/MTS OCEANS Conference and Exhibition*, pages 1–7, 2016.

[24] K. Skinner and M. Johnson-Roberson. Towards real-time underwater 3d reconstruction with plenoptic cameras. In *Proceedings of the IEEE/RSJ International Conference on Intelligent Robots and Systems*, pages 2014–2021, 2016.

[25] M. Tao, P. Srinivasa, J. Malik, S. Rusinkiewicz, and R. Ramamoorthi. Depth from shading, defocus, and correspondence using light-field angular coherence. In *Proceedings of the IEEE Conference on Computer Vision and Pattern Recognition*, pages 1940–1948, 2015.

[26] C. Tsiotsios, M. E. Angelopoulou, A. J. Davison, and T.-K. Kim. Effective backscatter approximation for photometry in murky water. *arXiv:1604.08789*, 2016.

[27] S. Wanner and B. Goldluecke. Variational light field analysis for disparity estimation and super-resolution. *IEEE Transactions on Pattern Analysis and Machine Intelligence*, 36(3):606–619, March 2014.

[28] J. Zhang, Y. Cao, and Z. Wang. Nighttime haze removal with illumination correction. *CoRR*, abs/1606.01460, 2016.